Phyllosilicate mineral assemblages of the SAFOD Pilot Hole and comparison with an exhumed segment of the San Andreas Fault System

John G. Solum and Ben A. van der Pluijm

Department of Geological Sciences, University of Michigan, Ann Arbor, Michigan, USA

Received 7 March 2004; accepted 24 March 2004; published 24 June 2004.

[1] This paper establishes a reference phyllosilicate data set from the SAFOD Pilot Hole for future SAFOD drilling and presents an application of these data for studies of exhumed fault segments. The chlorite assemblages in cuttings from two intervals of the SAFOD Pilot Hole are separated into two populations based on X-ray diffraction characteristics. The first population is found in granite in both the deeper and shallower interval, whereas the second population occurs only in clastic sedimentary rocks in the shallower interval. The characteristics of the first population match those for protolith and cataclasite of the exhumed Punchbowl Fault, whereas samples from intensely deformed ultracataclasite are most similar to the second. This supports previous findings that the mineral assemblages in the ultracataclasite formed after the cessation of motion along the fault, above a depth of ~2 km, and that mineral assemblages in these exhumed fault rocks have been overprinted by post-faulting alteration. *INDEX TERMS:* 3625 Mineralogy and Petrology: Descriptive mineralogy; 3694 Mineralogy and Petrology: Instruments and techniques; 8010 Structural Geology: Fractures and faults; 8159 Tectonophysics: Rheology—crust and lithosphere. **Citation:** Solum, J. G., and B. A. van der Pluijm (2004), Phyllosilicate mineral assemblages of the SAFOD Pilot Hole and comparison with an exhumed segment of the San Andreas Fault System, *Geophys. Res. Lett.*, *31*, L15S19, doi:10.1029/2004GL019909.

1. Introduction

[2] Mechanically weak fault behavior [e.g., *Lachenbruch and Sass*, 1980; *Zoback*, 2000], has been attributed to the presence of phyllosilicates in fault zones as neoformed clays either directly weaken faults due to low strength [e.g., *Wang*, 1984] or influence the permeability structure of fault zones [e.g., *Morrow et al.*, 1984; *Zhang et al.*, 1999; *Zhang and Cox*, 2000; *Faulkner and Rutter*, 2001]. Chlorite, the dominant phyllosilicate observed in the Pilot Hole, is found in other fault zones, such as the exhumed Punchbowl Fault [e.g., *Chester and Logan*, 1986; *Schulz and Evans*, 1998; *Solum et al.*, 2003], and at depth along the active Nojima Fault [e.g., *Ohtani et al.*, 2000]. Exhumed fault zones have been used to study the effectiveness of fault weakening mechanisms [e.g., *Chester and Logan*, 1986; *Evans and Chester*, 1995; *Vrolijk and van der Pluijm*, 1999; *Faulkner and Rutter*, 2001; *Solum et al.*, 2003], but samples from drilled active faults provide unique opportunities to determine in situ characteristics of fault rocks prior to exhumation. By providing samples from depth, the SAFOD Pilot Hole (SPH) provides the necessary baseline for future studies of fault rocks from the main SAFOD hole, but also permits comparison with exhumed fault segments, such as the Punchbowl Fault (PBF) (Table 1).

[3] The protoliths of the PBF are quartz diorite, quartz monzonite, mica schist, and arkosic fluvial sandstone/siltstone with conglomeratic interlayers, as well as shallow marine arkosic sandstone with conglomerate lenses. This is similar to the rocks of the SPH, consisting of granite and shallow marine coarse sandstones. Thus, it is possible to directly compare characterizations of phyllosilicates from both localities (Figure 1).

2. Experimental Methods

2.1. Sample Description

[4] Cuttings were collected from two intervals from the SPH (488–914 m and 1585–2012 m). These intervals were based on results of point counts (M. Rymer, personal communication, 2004), and were chosen to include the transition from granite to sedimentary cover at ~760 m, as well as zones of chloritic alteration within the granite, including a shear zone at ~1800 m [*Boness and Zoback*, 2004].

2.2. X-Ray Diffraction

[5] The cuttings were analyzed using oriented and random sample preparations. Oriented preparations were used to enhance the intensities of (00l) peaks, aiding in the identification of phyllosilicate phases. Both bulk and clay (<5 μm) fractions were analyzed for each sample. Oriented samples were prepared by placing a clay-water slurry on a glass slide and allowing it to dry. Random samples were prepared using an end-packing device [*Moore and Reynolds*, 1997]. Samples of bentonite drilling mud and barite mud additive were analyzed in order to recognize contamination by those materials in the cuttings (Figure 2). Peaks on powder patterns from cuttings that overlap with peaks from drilling mud were not used in samples containing significant traces of drilling mud.

[6] Samples were analyzed using a Scintag X1 θ–θ powder diffractometer, with an accelerating voltage of 35.0 kV and a filament current of 20.0 mA. Oriented samples were scanned from 2–30°2θ at a scan rate of 0.25°/min, and random samples from 4–40°2θ at a rate of 1.0°/min.

[7] Bulk samples with oriented preparations were analyzed in order to determine relative mineral concentrations (Figure 3). The area of each relevant peak on an individual powder pattern was measured, and the area of that peak

Copyright 2004 by the American Geophysical Union.
0094-8276/04/2004GL019909

Table 1. Relative Mineral Concentrations From the Safod Pilot Hole Based on XRD of Bulk Samples With Oriented Preparations[a]

Depth (ft)	Depth (m)	Normalized Relative Area										
		i/m/b	lmt	hbl	c-s	stlb	chl	al	qtz	kfs	ep	cal
1600	487.7	0.32	0	0	0.31	0	0.05	0	0.75	0.78	0	0
1700	518.2	0.52	0	0	0.75	0	0.09	0	0.63	0.57	0	0
1800	548.6	0.54	0	0	1.00	0	0.12	0	0.32	0.70	0	0
1900	579.1	0.69	0	0	0.66	0	0.18	0	0.47	0.54	0	0
2000	609.6	0.31	0	0	0.34	0	0.21	0	0.34	1.00	0	0
2100	640.1	0.19	0	0	0.11	0	1.00	0	0.93	0.06	0	0
2200	670.6	0.57	0	0	0.44	0	0	0	0.44	0.87	0	0
2300	701.0	0.38	0.06	0	0	0	0	0	1.00	0.63	0	0
2400	731.5	0.23	0.04	0	0.24	0	0	0	0.72	0.86	0	0.10
2500	762.0	0.50	0.10	0	0.78	0	0	0	0.34	0.62	0	0.31
2600	792.5	1.00	0.13	0	0	0	0.15	0	0.53	0.28	0	0.39
2700	823.0	0.23	0.49	0	0	0	0.15	0	0.49	0.45	0	0.68
2800	853.4	0.36	0.03	0	0	0	0.65	0	0.40	0.27	0	1.00
2900	883.9	0.26	0.16	0	0	0	0.17	0	0.61	0.64	0	0.51
3000	914.4	0.41	0.14	0	0	1.00	0.20	0	0.54	0.58	0	0
5200	1585.0	0	0.77	1.00	0	0	0.42	0.71	0.42	0.29	0	0
5300	1615.4	0.15	0.77	0.10	0	0	0.38	0.98	0.40	0.27	0	0
5400	1645.9	0.26	0.95	0.00	0	0	0.28	0.52	0.25	0.35	0	0
5500	1676.4	0	1.00	0.21	0	0	0.21	0.61	0.40	0.38	0	0
5600	1706.9	0.05	0.67	0.29	0	0	0.39	0.62	0.46	0.41	0	0
5700	1737.4	0.13	0.79	0.39	0	0	0.18	0.81	0.42	0.40	0.49	0
5800	1767.8	0.10	0.89	0.52	0	0	0.13	1.00	0.35	0.39	1.00	0
5900	1798.3	0.15	0.66	0.68	0	0	0.22	0.75	0.36	0.49	0.74	0
6000	1828.8	0.10	0.87	0.53	0	0	0.18	0.76	0.29	0.48	0	0
6100	1859.3	0.34	0.89	0.25	0	0	0.37	0.47	0.27	0.25	0	0
6200	1889.8	0.33	0.46	0.14	0	0	0.27	0.52	0.27	0.66	0	0
6300	1920.2	0.20	0.62	0.14	0	0	0.26	0.53	0.31	0.60	0	0
6400	1950.7	0.28	0.45	0.15	0	0	0.25	0.64	0.32	0.66	0	0
6500	1981.2	0.42	0.59	0.32	0	0	0.27	0.50	0.26	0.49	0	0
6600	2011.7	0.14	0.63	0.27	0	0	0.13	0.62	0.41	0.62	0	0

[a]The area of each relevant peak on an individual powder pattern was measured, and the area of that peak relative to the sum of the analyzed peaks from that sample was calculated. These relative areas were normalized to the largest relative area for a particular mineral. The phases that were analyzed are undifferentiated illite/biotite/muscovite (i/b/m) (8.8°2θ), laumontite (lmt) (9.3°2θ), stilbite (stlb) (9.7°2θ), hornblende (hbl) (10.5°2θ), mixed layer chlorite-smectite (C-S) (~10.6°2θ), chlorite (chl) (12.4°2θ), albite (ab) (13.8°2θ), quartz (qtz) (20.8°2θ), K-spar (kfs) (27.5°2θ), epidote (ep) (15.8°2θ), and calcite (cal) (29.5°2θ). All values of 2θ are for CuKα radiation. The contact between granite and overlying clastic sedimentary rock is ~760 m. Variations in phyllosilicates are discussed in the text. The differences between the shallow and deep granite are due to 1) possible weathering/alteration of the granite before or during deposition of the overlying clastic rocks and 2) the greater abundance of drilling mud in the shallower granite samples, which can increase the background on XRD powder diffraction patterns, making the peaks used to quantify albite and hornblende difficult to measure. Therefore a value of zero is best interpreted as "below detection limits", which are on the order of a few weight percent.

relative to the sum of the analyzed peaks from that sample was calculated. These relative areas were normalized to the largest relative area for a particular mineral. The phases that were analyzed are undifferentiated illite/biotite/muscovite (8.8°2θ), mixed layer chlorite-smectite (C-S) (~10.6°2θ), and chlorite (12.4°2θ). Measured but unreported phases are quartz, K-spar, hornblende and albite. In addition, one sample from 914 m depth contains stilbite, three samples from 1737–1798 m contain epidote, and six samples from 488–914 m contain calcite. The chlorite (001) peak at 6.2°2θ or the C-S 001 peak at ~5.2–5.4°2θ were not used as the bentonite drilling mud has a peak in that range, except for samples with very little or no contamination. Clay fractions with random orientations (Figure 4) were analyzed in order to determine the composition of chlorite as discussed below. Tabulated relative mineral concentrations are shown in Table 1.

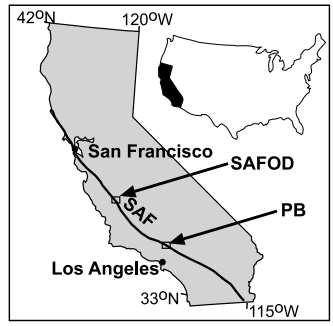

Figure 1. Location map of the SAFOD Pilot Hole (SAFOD) and the Punchbowl Fault (PB). SAF denotes the San Andreas Fault.

3. Results

3.1. Relative Mineral Concentrations

[8] Relative mineral concentrations in SPH samples are summarized in Figure 5. Chlorite is generally more common in the SPH granite samples, although there is one chlorite-rich sample in the SPH sedimentary cover. C-S is common in the shallow SPH sedimentary rocks that overlie the granitic protolith, and is absent in the granite; an indication that C-S in the SPH is associated with shallow reaction processes. Similar C-S in ultracataclasite from the PBF was interpreted as a post-faulting product [*Solum et al.*, 2003]. It should be noted that fault-related C-S does occur in the PBF, however it is morphologically different from post-faulting C-S and contains few smectite interlayers [*Solum et al.*, 2003].

3.2. Crystallinity

[9] Variation in the width of the (001) chlorite/C-S peak from XRD powder patterns for SPH samples are shown in Figure 6a, while results across the PBF are shown for comparison in Figure 6b [*Solum et al.*, 2003]. In the SPH, peaks are narrower in the granite and broader in the shallower sandstone, reflecting the decreasing abundance of smectite interlayers in those samples. Ultracataclasite in the PBF is also characterized by broad peaks, which are due to both a large number of smectite interlayers and small grain size in those samples.

[10] Samples from the SPH granite correlate with cataclasite and crystalline protolith from the PBF, while ultracataclasite most closely correlates with shallower sed-

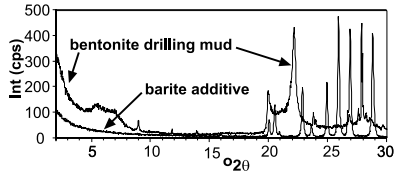

Figure 2. X-ray diffraction powder patterns for bentonite drilling mud and barite additive used to identify contamination on powder patterns of cuttings. Samples were glycolated and prepared with a preferred orientation.

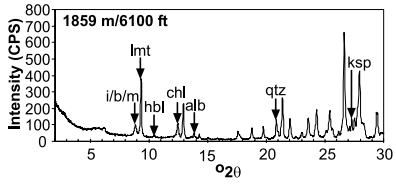

Figure 3. Representative powder patterns from glycolated bulk cutting samples prepared such that clays have a preferred orientation. The peaks are undifferentiated illite/biotite/muscovite (i/b/m), laumontite (lmt), hornblende (hbl), chlorite (chl), albite (alb), quartz (qtz), and K-feldspar (ksp). Unlabeled peaks are unused peaks from the phases mentioned in the preceding sentence, or drilling mud. The depths of the samples are indicated.

imentary rocks from the SPH. This further supports the interpretation that C-S observed in PBF ultracataclasite formed at a shallower depth than chlorite in the PBF cataclasite and protolith.

3.3. Chlorite and C-S Composition

[11] The populations of chlorite and C-S from the SPH and the PBF can be separated based on characteristics of the powder diffraction patterns. Figure 7a plots the width of the (002) chlorite/C-S peak (crystallinity) against the area of the (002) chlorite/C-S peak over the area of the (001) chlorite/C-S peak (the peak area ratio). Measurements were made using bulk samples with a preferred orientation. The peak area ratio is a function of the chemical composition of chlorite and C-S. The values for the phyllosilicates from the SPH granite overlap with the crystalline and sedimentary protolith and cataclasite from the PBF, both of which were interpreted as pre or synfaulting [*Solum et al.*, 2003]. The values for clays from PBF ultracataclasite do not plot with the SPH granite, and are most similar to the SPH clastic sedimentary rocks, supporting the interpretation that C-S in the exhumed PBF ultracataclasite formed at a shallower depth than the PBF protolith and cataclasite.

[12] X-ray powder diffraction patterns also offer a semi-quantitative estimate of the composition of chlorite, provided that randomly oriented samples are used [*Brown and Brindley*, 1980]. Figure 7b depicts Y (the total amount of Fe) and D (the symmetry of Fe distribution between the octahedral and hydroxide sheets), using the method of *Brown and Brindley* [1980]. Only values from the deeper granite samples from the SPH are shown, as it was not possible to accurately measure the peak areas from

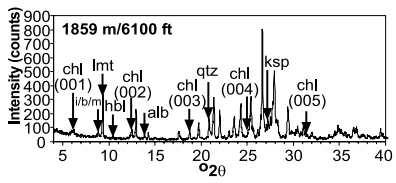

Figure 4. Representative powder patterns from the clay size fraction of cuttings prepared with a random orientation. Peak labels are the same as Figure 3, except that the (001) through (005) chlorite peaks are labeled, as these peaks are used to calculate the composition of the chlorite, as discussed in the text.

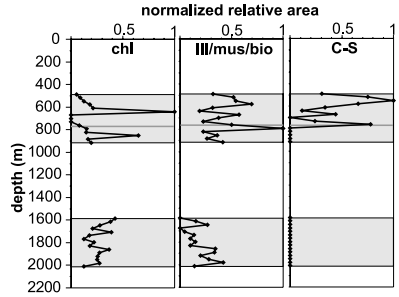

Figure 5. Relative mineral concentrations measured from powder patterns from glycolated, bulk samples. Abbreviations are the same as Figure 3. The contact between granite and overlying sediments is shown by a heavy gray line at a depth of ~760 m. Tabulated data, including non-phyllosilicates, can be found in Table 1.

shallower samples due to contamination by the drilling mud. Analogous to crystallinity data above, the composition of chlorite from the deeper SPH granite generally matches the composition of chlorite from crystalline and sedimentary

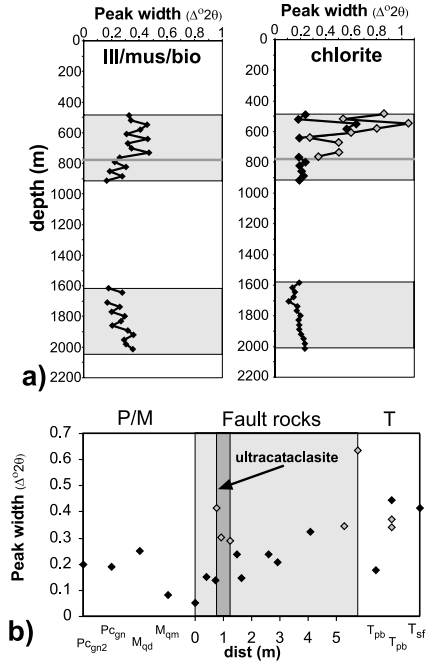

Figure 6. Crystallinity data from the SAFOD Pilot Hole (a) and the Punchbowl Fault (b). The values from the Punchbowl Fault are shown on a schematic cross section through the fault zone with zero arbitrarily set to the contact between Precambrian/Mesozoic protolith and the fault zone. The labeled zones are Precambrian/Mesozoic protolith (P/M), fault rocks, and Tertiary protolith (T). Samples of protolith that were not encountered along the traverse but that are exposed in the area are placed on the far right and far left of the diagram. Protoliths are Precambrian gneiss (Pcgn and Pcgn2), Mesozoic quartz diorite (Mqd), Mesozoic quartz monzonite (Mqm), Tertiary Punchbowl Formation (Tpb), and Tertiary San Francisquito Formation (Tsf). Black symbols are chlorite; gray symbols are chlorite-smectite.

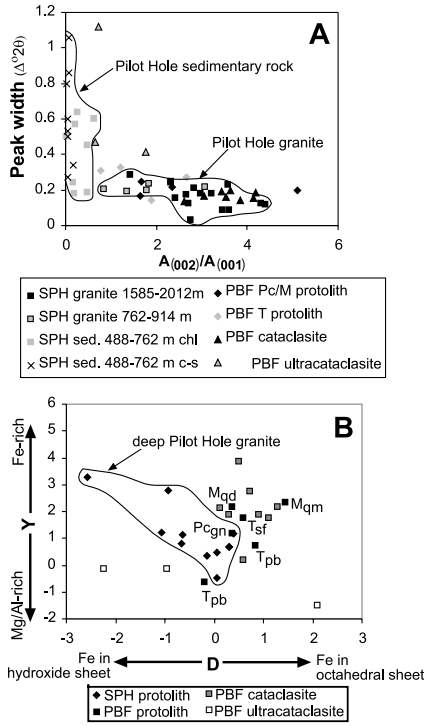

Figure 7. (a) Peak width vs. the area of the (002) chlorite peak over the area of the (001) chlorite peak from glycolated, bulk samples with an oriented preparation. (b) Y (total number of iron atoms in a unit cell) vs. D (anisotropy of iron distribution). The shallow section of the Pilot Hole is not shown due to contamination from the drilling mud. The unrealistic values of $Y < 0$ are most likely due to the presence of smectite interlayers, which influence peak areas. Abbreviations are defined in caption of Figure 6. PH granite refers to granite from the Pilot Hole and while PH sed. chl. refers to chlorite in sedimentary rock and PH sed. c-s refers to C-S in sedimentary rock from the Pilot Hole.

PBF protolith and PBF cataclasite, whereas the composition of PBF ultracataclasite does not.

4. Conclusions

[13] The primary objectives of this short paper are to establish a reference phyllosilicate data set for future SAFOD drilling, as well as for studies of exhumed fault zones, and, secondarily, to offer an application of this data set by comparing it with the Punchbowl Fault. Relative mineral concentrations, crystallinity, and chlorite composition all indicate that clays from the SPH granite correlate with PBF crystalline and sedimentary protolith and PBF cataclasite, while clays from PBF ultracataclasite most closely resemble the SPH clastic sedimentary rocks. These observations are compatible with the idea that the pre and syntectonic clays in the PBF protolith and PBF cataclasite formed while the fault was active, and therefore at a depth of 2–4 km [*Chester and Logan*, 1986], whereas clays in the exhumed ultracataclasite, representing the most intensely deformed fault rock formed at a shallower depth (<2 km). This is compatible with the earlier interpretation from microstructural work that clays in ultracataclasite are the result of postfaulting alteration [*Solum et al.*, 2003].

[14] The effects of post-faulting alteration limit inferences about fault behavior that can be made from exhumed rocks. Samples from boreholes that collect unaltered fault rocks, therefore, are required to constrain interpretations on the potential role of clays in fault mechanics. The Pilot Hole mineralogical data presented here provide the necessary reference data for comparison between protolith and fault rocks for planned sampling in the next phase of SAFOD, which will include collection of both cuttings and core, allowing for a more thorough characterization of fault-related mineral transformations and, through comparison with exhumed faults, the effects of postfaulting alteration on fault zones.

[15] **Acknowledgments.** Funding for this study was provided from NSF grant EAR-0230055 (BvdP) and an internship from DOSECC Inc. to Solum. The authors thank Steve Hickman and Jim Evans for their help in obtaining samples from the Pilot Hole and Liz Langenburg and Mike Rymer for providing point counts of the cultings. Constructive reviews by two anonymous reviewers helped to clarify the presentation and interpretation of the data.

References

Boness, N. L., and M. D. Zoback (2004), Stress-induced seismic velocity anisotropy and physical properties in the SAFOD Pilot Hole in Parkfield, CA, *Geophys. Res. Lett.*, *31*, L15S17, doi:10.1029/2004GL019020.

Brown, G., and G. W. Brindley (1980), X-ray diffraction procedures for clay mineral identification, in *Crystal Structures of Clay Minerals and Their X-ray Identification*, edited by G. W. Brindley and G. Brown, 305–359, Mineral. Soc., London.

Chester, F. M., and J. M. Logan (1986), Implications for mechanical properties of brittle faults from observations of the Punchbowl Fault zone, California, *Pure Appl. Geophys.*, *124*, 79–106.

Evans, J. P., and F. M. Chester (1995), Fluid-rock interaction in faults of the San Andreas system: Inferences from San Gabriel Fault rock geochemistry and microstructures, *J. Geophys. Res.*, *100*, 13,007–13,020.

Faulkner, D. R., and E. H. Rutter (2001), Can the maintenance of overpressured fluids in large strike-slip fault zones explain their apparent weakness?, *Geology*, *29*, 503–506.

Lachenbruch, A. H., and J. H. Sass (1980), Heat flow and energetics of the San Andreas Fault zone, *J. Geophys. Res.*, *85*, 6185–6222.

Moore, D. M., and R. C. Reynolds Jr. (1997), *X-ray Diffraction and the Identification and Analysis of Clay Minerals*, 378 pp., Oxford Univ. Press, New York.

Morrow, C. A., L. Q. Shi, and J. D. Byerlee (1984), Permeability of fault gouge under confining pressure and shear stress, *J. Geophys. Res.*, *89*, 3193–3200.

Ohtani, T., K. Fujimoto, H. Ito, H. Tanaka, N. Tomida, and T. Higuchi (2000), Fault rocks and past to recent fluid characteristics from the borehole survey of the Nojima Fault ruptured in the 1995 Kobe earthquake, Southwest Japan, *J. Geophys. Res.*, *105*, 16,161–16,171.

Schulz, S. E., and J. P. Evans (1998), Spatial variability in microscopic deformation and composition of the Punchbowl Fault, southern California: Implications for mechanisms, fluid-rock interaction, and fault morphology, *Tectonophysics*, *295*, 223–244.

Solum, J. G., B. A. van der Pluijm, D. R. Peacor, and L. N. Warr (2003), Influence of phyllosilicate mineral assemblages, fabrics, and fluids on the behavior of the Punchbowl Fault, southern California, *J. Geophys. Res.*, *108*(B5), 2233, doi:10.1029/2002JB001858.

Vrolijk, P., and B. A. van der Pluijm (1999), Clay gouge, *J. Struct. Geol.*, *21*, 1039–1048.

Wang, C.-Y. (1984), On the constitution of the San Andreas Fault zone in central California, *J. Geophys. Res.*, *89*, 5858–5866.

Zhang, S., and S. F. Cox (2000), Enhancement of fluid permeability during shear deformation of a synthetic mud, *J. Struct. Geol.*, *22*, 1385–1393.

Zhang, S., T. E. Tullis, and V. J. Scruggs (1999), Permeability anisotropy and pressure dependency of permeability in experimentally sheared gouge materials, *J. Struct. Geol.*, *21*, 795–806.

Zoback, M. D. (2000), Strength of the San Andreas Fault, *Nature*, *405*, 31–32.

J. G. Solum and B. A. van der Pluijm, Department of Geological Sciences, University of Michigan, 425 E. University Ave., 2534 C. C. Little Bldg., Ann Arbor, MI 48109-1063, USA. (jsolum@umich.edu)